VOL. 05 NO. 9,
AUGUST, 2024
E-ISSN 3026-958X
P-ISSN 3027-1169

African Scholar Publications & Research International
www.africanscholarpub.com

Journal of Science Innovation & Technology Research (JSITR)

Evaluation of Gabor Filter, GLCM, and DWT Performance in Brain Tumour Classification

Fausat Fadeke Agboola[1]; Wasiu Oladimeji Ismaila[2]; Oluyinka Iyabo Omotosho[2]; Adeleye Samuel Falohun[3]; & Folasade Muibat Ismaila[4]

[1]Department of Computer Science, Faculty of Physical Sciences, Modibbo Adama University, Yola, Adamawa State, Nigeria. [2]Department of Computer Science, Faculty of Computing and Informatics, Ladoke Akintola University of Technology, Ogbomoso, Oyo State, Nigeria. [3]Department of Computer Engineering, Faculty of Engineering and Technology, Ladoke Akintola University of Technology, Ogbomoso, Oyo State, Nigeria. [4]Department of Computer Science, Osun State Polytechnic, Iree, Osun State, Nigeria.

Abstract

The brain, vital for body function, can be afflicted by tumours, potentially leading to death or uncontrolled growth, and metastases if left untreated. Hence, automated classification of brain tumour types is crucial for faster treatment, better planning, and patient survival, as manual diagnosis of brain tumour types heavily relies on the expertise and sensitivity of radiologists. Thus, this paper evaluates the performance of Gabor filter, Gray Level Co-occurrence Matrix (GLCM), and Discrete Wavelet Transform (DWT) in identifying normal and abnormal brain tumours using four categories of brain MRI tumours from the Kaggle database. The performance analysis focuses on binary classification to determine the efficacy of each feature extraction method. The study found that Gabor features had a False Positive Rate (FPR) of 7.61%, False Negative Rate (FNR) of 8.57%, sensitivity of 91.43%, precision of 81.36%, and accuracy of 92.13% at 985.34 seconds. GLCM features had an FPR of 9.69%, FNR of 9.52%, sensitivity of 90.48%, precision of 77.24%, and accuracy of 90.36% at 364.74 seconds. DWT features had an FPR of 11.42%, FNR of 11.43%, sensitivity of 88.57%, precision of 73.81%, and accuracy of 88.58% at 275.53 seconds. The GLCM yielded most efficient feature extractor, which can serve as a useful technique and second reader to radiologists in diagnosing a brain tumour to reduce the mortality rate.

Keywords: Gabor filter, GLCM, DWT, MRI images, Brain tumour, Classification.

Introduction

Brain tumours are a type of illness that originates within the brain when irregular cells undergo uncontrolled and unrestricted growth, disregarding the usual regulations of cell division. This unchecked proliferation of abnormal cells can lead to their expansion both within and beyond the brain structure, potentially resulting in a life-threatening

condition if left untreated, eventually leading to the formation of metastases (Kaifi, 2023). Brain tumours represent a significant cause of mortality among teenagers and adults on a global scale (Yamasaki, 2022). However, advancements in diagnostic capabilities and the effectiveness of treatments have led to a reduction in mortality rates Sung *et al.* (2021). Despite this progress, there is still much work to be done to address the ongoing challenges associated with cancer.

Brain tumours are categorised into two primary types: primary and metastatic tumors. Primary tumours originate within the brain itself and include various subtypes such as meningioma, glioma, pituitary tumours, astrocytoma, acoustic neuroma, medulloblastoma, and others. On the other hand, metastatic tumours commence outside the brain and rapidly spread to the brain from other parts of the body. Examples of metastatic tumours encompass those originating from breast cancer, cervical cancer, skin cancer, lung cancer, womb cancer, and ovarian cancer. These tumors can cause significant damage to the brain and can be difficult to treat. Metastatic brain tumours are more common than primary brain tumours, and the treatment approach depends on the type of tissue from which the original tumour originated (Balestrino *et al.*, 2020). Therefore, detecting brain tumours quickly is crucial and paves the way for further investigation.

Magnetic Resonance Imaging (MRI) serves as the initial diagnostic step for detecting brain tumours and precisely pinpointing their location, creating computerised images of the brain and spinal cord, which is commonly referred to as a scan or imaging modality. MRI is an essential tool for accurate diagnosis, treatment planning, and disease monitoring, offering detailed information on brain anatomy, cellular structure, and vascular supply. While an MRI image of a brain tumour may appear relatively straightforward, physicians often require quantitative data on the tumour's size and extent for further treatment decisions. In such cases, computer-based image processing techniques prove invaluable in analysing the tumour's dimensions (Abdusalomov *et al.*, 2023).

Related Work

Numerous techniques for extracting textural features have been suggested to identify, segment, and categorize brain tumours using MRI across different tissues, some of which are examined in this investigation. Harati *et al.* (2011) devised a computer-assisted classification approach merging conventional MRI with perfusion MRI across various diagnoses. Their method extracted features such as tumour shape, intensity characteristics, and rotation-invariant texture features. Through leave-one-out cross-validation on 102 brain tumours, the binary SVM classification yielded accuracy, sensitivity, and specificity rates of 87%, 89%, and 79%, respectively, for discriminating metastases from gliomas and 87%, 83%, and 96%, respectively, for discriminating high-grade from low-grade neoplasms. These findings underscore the efficacy of their approach in accurately discerning between different types and grades of brain tumours.

Zanaty (2012) introduced a hybrid approach that integrates fuzzy clustering, seed region growing, and Jaccard similarity coefficient algorithms to quantify gray matter (GM) and white matter (WM) volumes from MRI scans. This method uses both intensity data and anatomical data to divide MRIs into different tissues, noise, and differences in intensity that come from

fake brain images. Being able to get an average segmentation score of 90% at noise levels of 3% and 9% shows that this method is more reliable at separating areas, especially when medical imaging data has a low signal-to-noise ratio.

Biratu *et al.* (2021) employed a dataset comprising meningioma, glioma, and pituitary brain tumor types captured in axial, sagittal, and coronal anatomical views. Preprocessing involved normalization and resizing of the images, which were augmented by 90 rotations and vertical flipping to expand the training dataset. They developed a custom CNN model trained using an Adam optimizer with a mini-batch size of 16 and validated using 10-fold cross-validation. The convolution layer weights were initialised using a Glorot initializer. Evaluation metrics included sensitivity, specificity, accuracy, precision, recall, and the F1-score. The achieved sensitivities for meningioma, glioma, and pituitary were 89.8%, respectively, indicating the CNN model's high accuracy in classifying brain tumour types.

Wisaeng and Sa-Ngiamvibool (2023) introduce a novel technique for brain tumour segmentation called fuzzy Otsu thresholding morphology (FOTM). Their approach involves modifying original MRI image histograms using a colour normalising preprocessing technique along with histogram specification. Results show that for gliomas, meningiomas, and pituitary tumours, the average accuracy indices are 93.77%, 94.32%, and 94.37%, respectively. These findings suggest that combining the preprocessing method with histogram specification can substantially enhance the accuracy of tumour classification.

Deepa *et al.* (2023) employed a novel hybrid optimisation approach to segment and classify brain tumors. They utilised CNN features for enhanced categorization. The proposed approach, called the Chronological Jaya Honey Badger Algorithm (CJHBA), trained a Deep Residual Network (DRN) using the Jaya algorithm, the Honey Badger Algorithm (HBA), and a chronological concept. This trained network was then used for classification, with the extracted features serving as input. The performance was evaluated using the BRATS 2018 and Figshare datasets, with the BRATS dataset achieving the highest accuracy, sensitivity, and specificity scores of 0.9210, 0.9313, and 0.9284, respectively.

Despite the extensive research efforts in the field of brain tumour detection and classification, ongoing studies persist due to the intricate structure of human brain tissues. The complexity of this structure, coupled with the time-consuming nature of existing algorithms, continues to pose significant challenges for researchers in this domain. Thus, researchers remain dedicated to finding innovative solutions that will revolutionise the field of brain tumour detection and classification. Each method comes with its own set of advantages and constraints, and their effectiveness may vary based on the brain tumour's type and location. So, the goal of this study is to see how well the Gabor filter, the Gray Level Co-occurrence Matrix (GLCM), and the Discrete Wavelet Transform (DWT) can tell the difference between brain tumours that are normal and ones that are not.

Materials and Methods

The brain MRI image datasets used in this study were acquired from the Kaggle website. The acquired brain MRI images were preprocessed as reported by Arulogun *et al.* (2016) with little modification. The brain MRI images underwent preprocessing to remove noise and unwanted

elements. Contrast Limited Adaptive Histogram Equalisation (CLAHE) was applied for normalisation, ensuring a consistent representation of the images. Fuzzy C-means clustering was then utilised for segmentation. The segmented images were extracted using Gabor filters, GLCM, and DWT. Each of the extracted features were normalised using the min-max technique. The normalised feature was fused and combined using a modified CSO. Finally, classification was done by applying SVM to normal or abnormal classification. The evaluated results are based on four (4) categories of brain MRI images, gliomas, meningiomas, non-tumorous regions, and pituitaries. The workflow is shown in Figure 1.

Image acquisition

This phase involves the acquisition of MRI images from the Kaggle website. The dataset comprises 394 MR images categorized into four classes. There are 100 MR images of gliomas, 115 of meningiomas, 105 of non-tumorous regions, and 74 of pituitaries. Due to this initial imbalance, we employed a data augmentation method to rectify it. In Figure 2, a selection of MRI samples from the dataset is depicted, showcasing examples from each class.

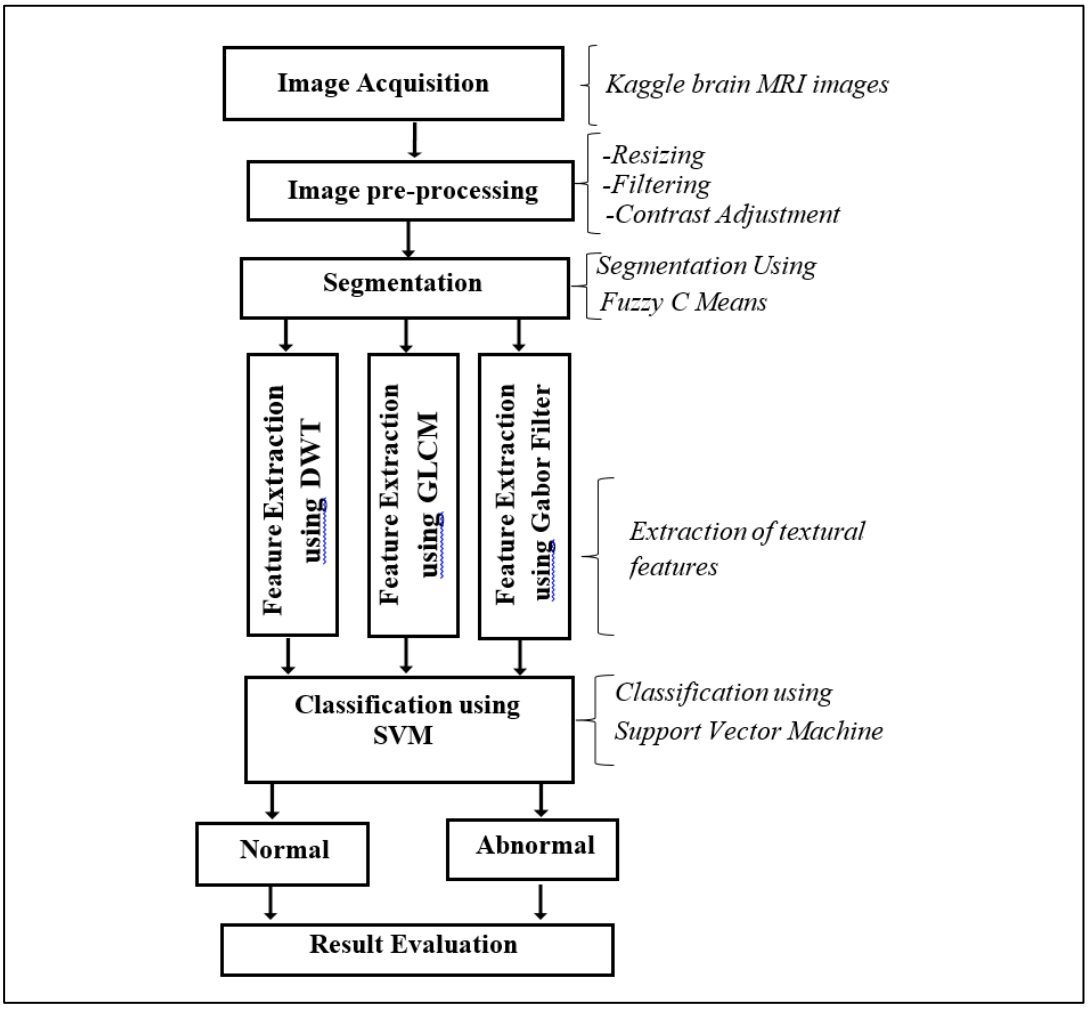


Figure1: The diagram illustrating the methodology and workflow

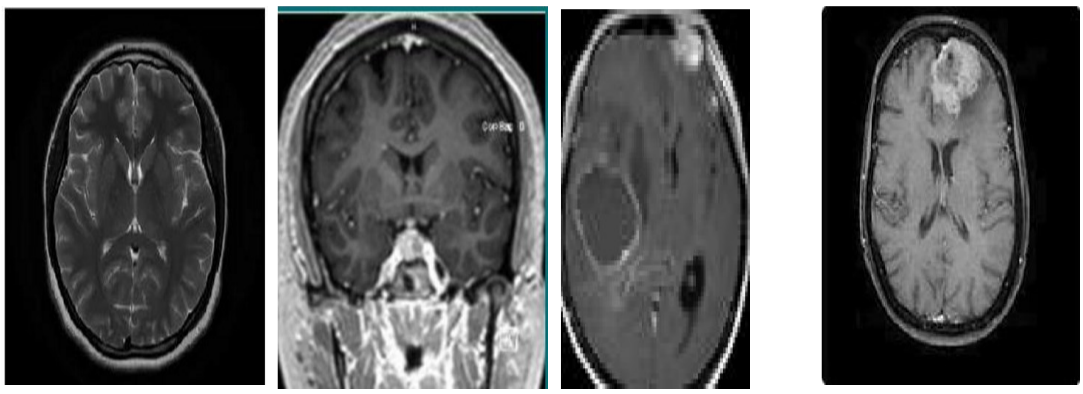


Figure 2. Acquired images of brain tumour from Kaggle data base

Image preprocessing

The acquired images underwent various preprocessing techniques, including resizing to uniform pixel dimensions and conversion to grayscale. Moreover, due to factors such as faulty switching and environmental conditions, impulse noise often affects a significant portion of MRI images. Therefore, noise filtering was applied. Filtering in image processing serves the primary purpose of achieving interpolation, noise reduction, and resampling. In this study, a combination of mean and median filters with different pixel values was employed to remove noise from MRI images. The median filter, specifically, was utilised to preserve image details at the edges while eliminating noise. This process involves scanning the images pixel by pixel and replacing each with the median value of its neighbouring pixels.

To address both intra-scan and inter-scan variations in MR image intensity, normalisation is essential following the identification of slices containing tumours. This normalisation process is crucial for enabling quantitative texture analysis. In this study, the histogram normalisation technique was utilised prior to conducting quantitative texture analysis. This method involves stretching and shifting the original image histogram to encompass all grayscale levels present in the image. It is defined as shown in Equation 1.

$$f(x,y) = \frac{I_{min} - I_{max}}{h_{max} - h_{min}} (h(x,y) - h_{min}) + I_{max} \quad (1)$$

where $h(x, y)$ represents the original histogram of the initial image, $f(x, y)$ denotes the new histogram, and h_{min} and h_{max} stand for the smallest and largest grayscale levels, respectively. I_{min} and I_{max} represent the new minimum and maximum intensity levels, respectively.

Image resized and converted to a grey-level image

The MRI scans obtained from the Kaggle database were stored in a database and subsequently converted into grayscale images with dimensions of 200 by 200. It is worth noting that the MRI scan images were originally considered to be colour intensity images with dimensions of 250 by 250, as depicted in Figure 3.

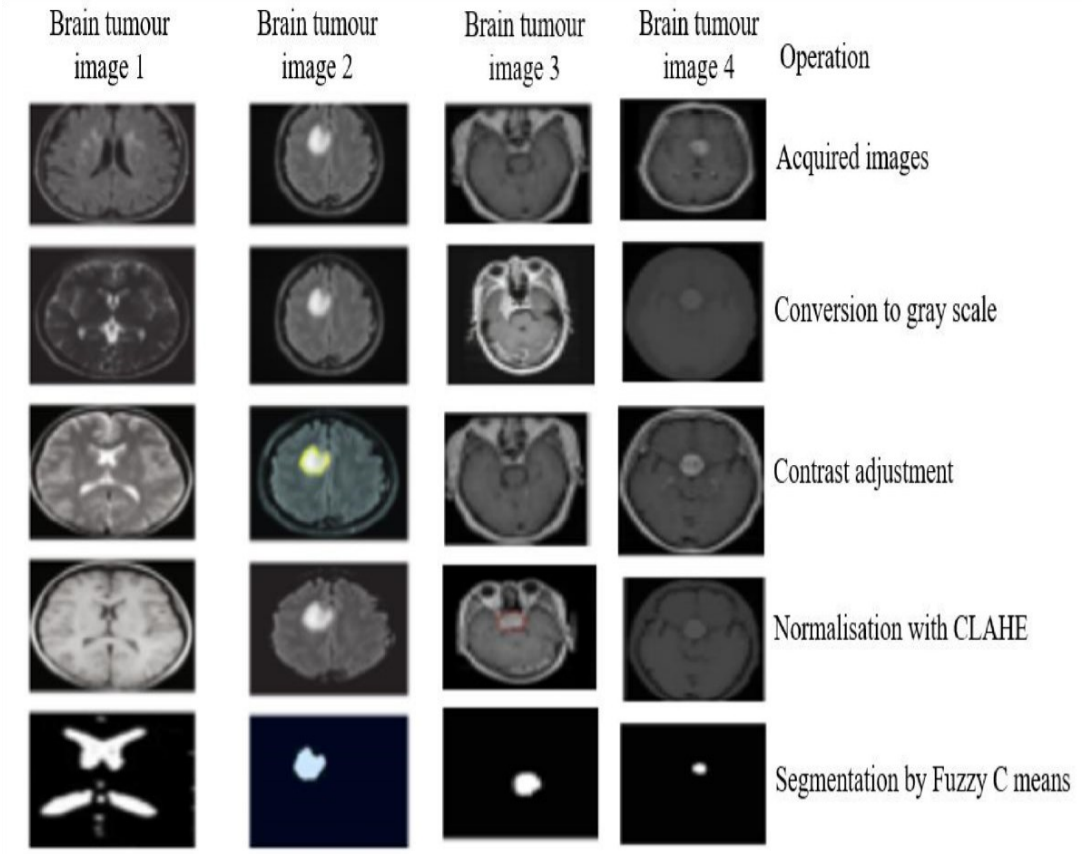


Figure 3: Pre-processing of the MRI brain tumour images: image 1 non tumour, image 2 Gliomas tumour, image 3 menigiomas tumour, image 4 pituatry tumour

Fuzzy C-Means (FCM) for Segmentation

The pre-treated images underwent segmentation using fuzzy C-means (FCM), a process that assigns labels to individual voxels in MRI images to denote their tissue characteristics and anatomical features. In tumour classification, the primary aim of region of interest (ROI) detection is to pinpoint the tumour area within an MRI scan, enhancing visualisation and enabling quantitative analysis of image structures during feature extraction. The algorithm outlined below illustrates the sequential steps involved in FCM image segmentation. Set the starting points for the cluster centers c_i and t = 0.

1. Initialize the fuzzy partition memberships functions μ_{ij} according to equation (2)

$$\mu_{ij} = \left(\sum_{m=1}^{C} \left(\frac{\|x_j - c_i\|}{(\|x_j - c_m\|)^{2/(k-1)}} \right) \right)^{-1} \quad (2)$$

2. Let $t = t + 1$ and compute new cluster centres $c_i$using equation (3).

$$c_i = \frac{\sum_{j=1}^{N} \mu_{ij}^{k} x_j}{\sum_{j=1}^{N} \mu_{ij}^{k}} \quad (3)$$

3. Repeat Steps 2 to 3 until convergence is noticed.

Feature Extraction

In this context, Gabor filters, GLCM, and DWT were utilised for this purpose. The extracted features from these techniques were combined to enhance the machine learning model's ability to distinguish between different classes. These features comprise statistical information about the detected brain tumour image, resulting in a set of six-value features.

Feature extraction using Gabor filter

The Gabor filter is primarily designed to be sensitive to the orientation of features in an image, responding strongly to specific frequencies and directions (Ismaila *et al.*, 2018).). In this study, the 2D Gabor filter, denoted as $H(x, y, \sigma x, \sigma y, f, \theta)$ was applied to the detected tumour image to produce a Gabor-filtered image $f(x, y)$. This filter breaks down the image into various scales (δ) and orientations (θ), effectively capturing spatial location, frequency, and orientation selectivity. The Gabor-filtered image is computed using Equations 4 and 5, as described below.

$$f(x,y) = \exp\left[-\frac{1}{2}\left(\left(\frac{x'}{\sigma_x}\right)^2 + \left(\frac{y'}{\sigma_y}\right)^2\right)\right] \times \cos(2\pi f x') * i(x,y) \qquad (4)$$

where

$$H(x,y,\sigma x,\sigma y,f,\theta) = \exp\left[-\frac{1}{2}\left(\left(\frac{x'}{\sigma_x}\right)^2 + \left(\frac{y'}{\sigma_y}\right)^2\right)\right] \times \cos(2\pi f x') \quad (5)$$

$$x' = \delta^{-m}(x\cos\theta + y\sin\theta)$$

$$y' = \delta^{-m}(y\cos\theta - x\sin\theta)$$

σ_x= complete basis, and = non-orthogonal basis of the Gabor filter.

In the decomposition of the detected tumour part; five orientations in [0, π]; $\theta = \{0^{\circ}, 45^{\circ}, 90^{\circ}, 135^{\circ}, 180^{\circ}\}$ with single scale =1 was used. This process resulted in the creation of five filters, each of size 5x1=5. These filters were used to generate five filtered images by concatenating each filter with the input image. Subsequently, 4x4 blocks were considered within each of the five filtered images, resulting in the creation of a column vector containing a total of 1x5x4x4 = 80 components from the input MRI image. This column vector was then normalised to have a zero mean and unit variance. Finally, this normalised column vector was utilised as an input for the normalisation module. **3.5.2. Feature extraction using DWT**

The discrete wavelet transform (DWT) offers an effective method for feature extraction by conducting multi-level decompositions of the image. In this study, a three-level 2-D DWT decomposition was employed to reduce the size of the image matrix, utilising the "Daubechies" filter. Each row of the image first received the wavelet transform treatment, and then each column of the final image from the first step received a similar treatment. The final sub-bands, namely LL3, LH3, HL3, and HH3, resulting from this process, were utilised for extracting statistical features. The approximation coefficient (LL), which contains the maximum information of the image, was extracted until the final round of decomposition (LL3) in the same manner as that of the original image. The output of the 2-D DWT technique was converted to a feature vector to become input to the normalization modules.

Feature extraction using Gary Level co-occurrence matrix (GLCM)

In this research, six textural characteristics were utilised, including angular second moment (energy), correlation, contrast, homogeneity, sum of the average (mean), and standard deviation. The Grey-Level Co-occurrence Matrix (GLCM) was computed for the four directions surrounding the pixel under examination. A sliding window of size 8 x 8 was used to facilitate the calculation of co-occurrence and the extraction of textural features. The six textural features from the cooccurrence matrices were analysed in four directions (0°, 45°, 90°, and 135°) with a distance of one (d = 1). Each sliding window produced 24 texture feature sets (4 directions x 1 distance x 6 texture features) computed from the GLCM. Additionally, six statistical features were computed using Equations 6 to 11.

1. Mean (M): The mean of an image is determined by summing up all the pixel values within the image and then dividing this sum by the total number of pixels in the image.

$$Mean\ \bar{x} = \frac{1}{N}\sum_{i=1}^{N} x_i \quad (6)$$

2. Standard Deviation (SD): The standard deviation, which is the second central moment, describes the probability distribution of an observed population and is defined as;

$$Standard\ deviation, s = \sqrt{\frac{1}{N-1}\sum_{i=1}^{N}(x_i - \bar{x})^2} \quad (7)$$

3. Energy (En): Energy refers to the measurable level of pixel pair repetitions within an image, serving as a metric for gauging image similarity. Similar to the angular second moment, energy is defined as;

$$Energy = \sum_{i,}(i,j)^2 \quad (8)$$

4. Contrast: Contrast quantifies the intensity difference between a pixel and its neighboring pixels across the entire image, and it is defined as;

$$Contrast = \sum_{i,}|i-j|^2\, p(i,j) \quad (9)$$

5. Homogeneity: Homogeneity assesses how closely distributed elements in the image cooccurrence matrix are to its diagonal elements. A higher value signifies a superior intensity level and enhanced contrast of the image edges. It is defined as;

$$Homogeneity = \sum_{i,j}\frac{p(i,j)}{1+|i-j|} \quad (10)$$

6. Correlation: Correlation quantifies the extent to which the intensity values of a pixel are linearly related to those of its neighbouring pixels. It offers data regarding the level of linearity present in the image.

$$Correlation = \sum_{i,j} p\,(i,j)\frac{(i-\mu i)(j-\mu j)}{\sigma_i \sigma_j} \quad (11)$$

Classification using Support Vector Machine (SVM)

SVM was adopted to classified the features that were extracted using Gabor filter, GLCM, and DWT techniques. A multiple binary classification problem was explored to achieve a multiclass classification for the four classes. Textural brain MRI features were classified into normal (no tumour) and abnormal. SVM classification predictions for the best hyperplane with the maximum margin was achieved using Equation 12.

$$g(x) = w^T x + w_0 = 0 \quad (12)$$

where x represents the feature descriptor, while w and w_0 represent unknown parameters obtained from training samples $\{(x_i, y_i)|1 \leq i \leq N\}$ (xi, yi),

where x_i and $y_i$denote the feature descriptor and the corresponding class label, respectively, with y_i belonging to either +1+1 or −1−1. The process involves solving an optimization problem rooted in big margin theory. After computing the best hyperplane, Equation 13 was used to classified a test sample x.

$$g(x) = \sum_{i=1}^{N_s} \lambda_i y_i x_i^T x + w_0 \quad (13)$$

In this equation,λ_i represents Lagrange multipliers, and N_s denotes the number of support vectors, which are the training samples corresponding to non-zero λ_i. The Kernel technique is applied when data samples from two classes cannot be separated linearly. The function g(x) is expressed as Equation 14 using a kernel function.

$$g(x) = \sum_{i=1}^{N_s} \lambda_i y_i K(x_i, x) + w_0 \quad (14)$$

In this context, (x_i, x) represents the kernel function, which calculates the inner product of the data. The parameter C, defined by the user, is used to control the penalty for misclassifications in the higher-dimensional space. This penalty or error, influenced by the kernel, is adjusted by the user-defined parameter C. In this study, the Radial Basis Function (RBF) kernel was employed, as depicted in Equation 15, with C set to 2000.

$$(x_i, x) = \exp(-\gamma \|x_i - x\|^2) \, , \gamma > 0 \quad (15)$$

The width of the kernel function is the γ. The RBF kernel now has two parameters γ and C.

Performance Evaluation Measures

The effectiveness of the analysed techniques was assessed by evaluating their recognition accuracy, False Positive Rate (FPR), False Negative Rate (FNR), precision, sensitivity, and computation time. These performance metrics were calculated using a confusion matrix, defined in Equations 16 to 20, which includes True Positive (TP), False Positive (FP), False Negative (FN), and True Negative (TN).

$$\text{False Positive Rate (FPR)} = \frac{\text{FP}}{\text{TN+FP}} \quad (16)$$

$$\text{False Negative Rate (FNR)} = \frac{\text{FN}}{\text{TP+FN}} \quad (17)$$

$$\text{Sensitivity} = \frac{\text{TP}}{\text{TP+FN}} \quad (18)$$

$$\text{Precision} = \frac{\text{TP}}{\text{TP+FP}} \quad (19)$$

$$\text{Accuracy} = \frac{\text{TP+TN}}{\text{TP+TN+FP+FN}} \quad (20)$$

where; TP represents the MR images correctly classified as brain tumours, TN represents the MR images correctly classified as the normal brain, FP represents the MR images of the normal brain classified as a tumour, and FN represents the MR images of brain tumours classified as normal.

Results and Discussion

Feature Extraction Table for Normal/Abnormal of Brain Tumour Images

The results in Table 1 show how well the Gabor Filter, GLCM, and DWT methods for feature extraction worked on images of both normal and abnormal brain tumours. Among the 394 brain tumour images analysed, 105 were classified as normal, while the remaining 289 were deemed abnormal. For the Gabor Filter technique, 96 normal brain datasets were accurately identified as normal, while 9 datasets were misclassified as abnormal. Additionally, 267 abnormal datasets were correctly classified, while 22 were incorrectly labelled as normal. Utilising the GLCM technique, 95 normal brain datasets were correctly classified, with 10 misclassified as abnormal. Regarding abnormal datasets, 261 were accurately identified, while 28 were incorrectly labelled as normal. In the case of the DWT technique, 93 normal brain datasets were correctly classified, while 12 were misclassified as abnormal. Furthermore, 256 abnormal datasets were accurately identified, while 33 were misclassified as normal. Overall, the Gabor filter technique showed higher accuracy in classifying both normal and abnormal brain datasets compared to the GLCM and DWT techniques. It correctly identified a higher number of normal datasets as normal and abnormal datasets as abnormal, with fewer misclassifications.

Table 1: Feature Extractions Table for Normal/Abnormal

Technique	**Actual Class**	**Predicted Class**	
		Normal	Abnormal
Gabor Filter	Normal (105)	95	10
	Abnormal (289)	28	261
GLCM	Normal (105)	95	10
	Abnormal (289)	28	261
DWT	Normal (105)	93	12
	Abnormal (289)	33	256

Evaluation Results for Normal/Abnormal Feature Extraction

Table 2 presents the results obtained by the Gabor Filter, GLCM, and DWT techniques concerning performance metrics for normal and abnormal brain images. The results obtainable in the table revealed that the Gabor features achieved an FPR of 7.61%, an FNR of 8.57%, a sensitivity of 91.43%, a precision of 81.36%, and an accuracy of 92.13% at 985.34 seconds. Also, GLCM features achieved an FPR of 9.69%, an FNR of 9.52%, a sensitivity of 90.48%, a precision of 77.24%, and an accuracy of 90.36% at 364.74 seconds. The DWT features achieved an FPR of 11.42%, an FNR of 11.43%, a sensitivity of 88.57%, a precision of 73.81%, and an accuracy of 88.58% at 275.53 seconds.

Based on Table 2, we can see that the GABOR filter, when compared to GLCM features, increased the normal/abnormal scheme FPR and FNR by 0.95 and 2.08 percent, respectively. It also increased the sensitivity, precision, and classification accuracy by 0.95 percent, 4.12 percent, and 1.7 percent, respectively. GLCM features also had better normal/abnormal classification sensitivity (1.96%), precision (3.43%), and accuracy (1.78%) compared to DWT

features. They also had lower rates of false positives and false negatives (1.73% and 1.9%, respectively). For the normal/abnormal scheme, Gabor Filter features outperformed DWT by a factor of 2.86, 7.55, and 3.55, respectively, while reducing the false positive rate (FPR) and false negative rate (FNR) by 3.81% and 2.83%, respectively. The Gabor Filter features improved the performance of the normal/abnormal scheme significantly. Additionally, the relatively low FPR and FNR values indicate that Gabor features have a high level of accuracy in distinguishing between normal and abnormal brain images.

Table 2: Performance features of GABOR Filter, GLCM and DWT

Technique	FPR	FNR	Sensitivity	Precision	Accuracy	Computation (s)
GABOR	7.61%	8.57%	91.43%	81.36%	92.13%	985.34
GLCM	9.69%	9.52%	90.48%	77.24%	90.36%	364.74
DWT	11.42%	11.43%	88.57%	73.81%	88.58%	275.53

It is inferred from the result achieved in this study that the Gabor filter has the highest computation time, followed by GLCM, while the DWT technique has the least computation time. With respect to computation time, DWT outperformed both Gabor and GLCM techniques, as shown in Figure 4. The findings of this study provide further evidence to support the claims made by Yılmaz and Bayrak (2019) and Mahmoud *et al.* (2008) regarding the superior computational efficiency of the DWT technique. These results highlight the potential of DWT for use in real-time applications where fast processing is crucial. In terms of processing speed, DWT is the most efficient and least computationally expensive of the three. Furthermore, the high computational time of Gabor features is due to the more inherent features in both the training and testing sets. This is in line with the submission of Raheja *et al.* (2013), who reported that the Gabor filter approach is computationally expensive.

Moreover, the results obtainable from Table 4.2 revealed that with Gabor features, there are minimal false positives and false negatives compared to GLCM and DWT features. This implies that there is minimal misclassification of the MRI brain dataset with the Gabor features. Hence, with reduced FPR and FNR from Gabor features, a more accurate brain tumour detection system can be achieved. This supported what Shanthi and Karthikeyan (2016) said, that the Gabor filter can cut down on false positives and negatives because it is good at using high-performance texture analysis for spatial frequency analysis in the extraction of MRI image features. The reduction in false positives and false negatives achieved by using Gabor features in brain tumour detection is crucial for improving the overall accuracy of the system. By accurately identifying and classifying brain tumours, medical professionals can make more informed decisions regarding treatment plans and patient care. Figures 5 and 6 depict the graph of the performance with respect to FNR and FPR.

Similarly, the Gabor filter technique outperformed both the GLCM and DWT techniques in terms of sensitivity, precision, and accuracy. This implies that the Gabor filter produces more discriminating features for the detection of tumours than GLCM and DWT techniques. These results suggest that incorporating the Gabor filter technique into the diagnostic process can significantly improve the accuracy and reliability of brain tumour detection. By leveraging its

superior performance in sensitivity, precision, and accuracy, medical professionals can enhance their ability to accurately identify and classify brain tumours, ultimately leading to better treatment outcomes for patients.

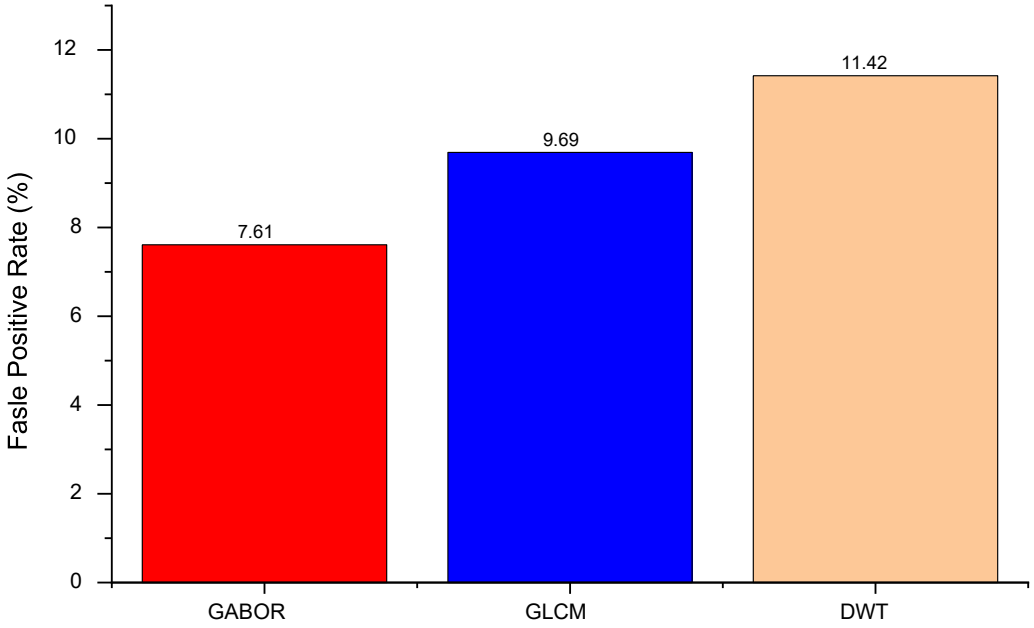


Figure 4: False Positive Rate Feature Extraction Techniques

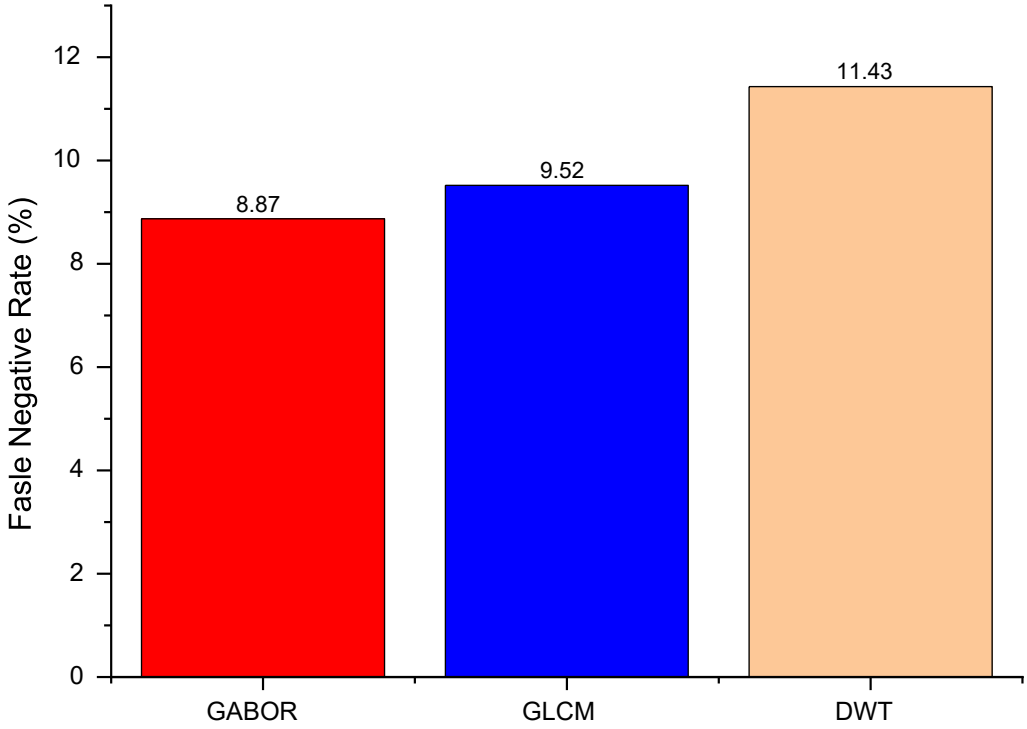


Figure 5: False Negative Rate Feature Extraction Techniques

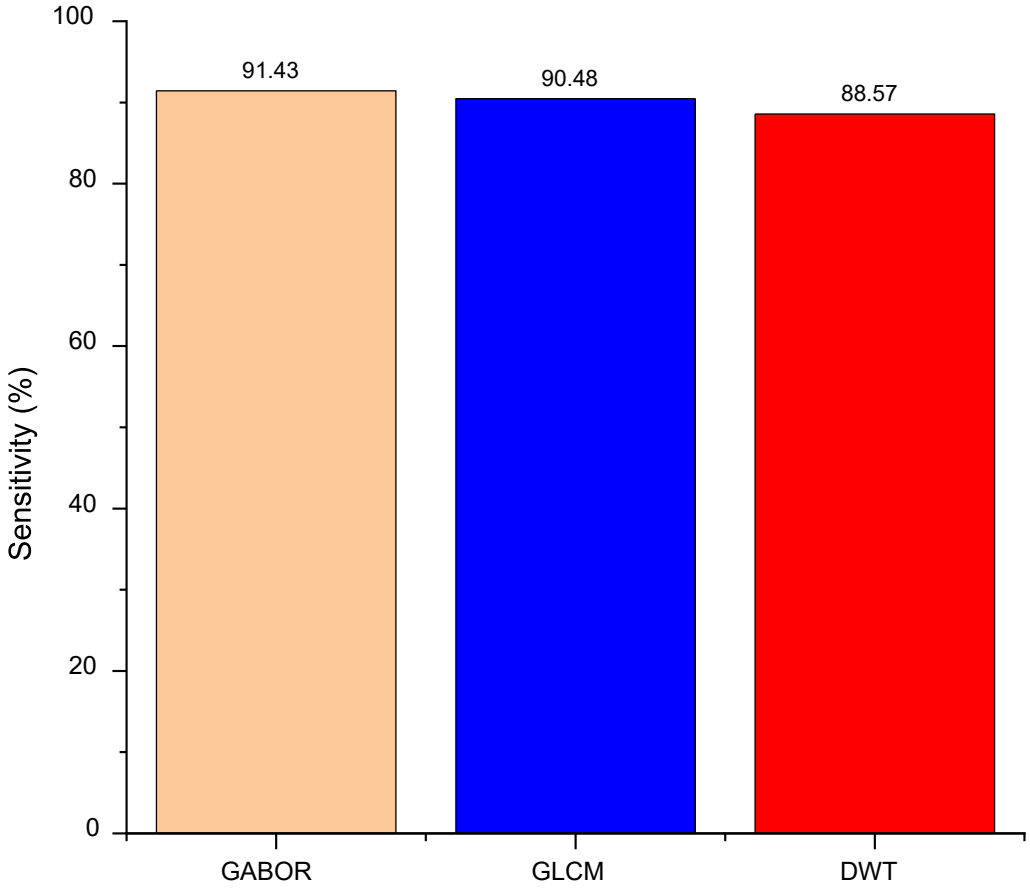


Figure 6: Sensitivity Feature Extraction Techniques

The DWT technique was the least performed among the others, despite the advantage of the reduction in computation. This may be attributed to the loss of discrimination power in the decomposition process. This is contrary to the submission of Thakral and Manhas (2018), who postulated that DWT reduces the size of an image without compromising on quality, and hence resolution increases. The loss of discrimination may be attributed to noise in the dataset. Also, the findings of Raheja *et al.* (2013) reveal that GLCM techniques outperformed the Gabor filter in terms of accuracy, which is contrary to the findings in this study. Figures 7, 8, and 9 depict the performance of the Gabor filter, GLCM, and DWT techniques in terms of sensitivity, precision, and accuracy.

The results of this pilot investigation suggest that Gabor filter features are better than GLCM and DWT in classifying MRI scans of brain tumours in terms of sensitivity, precision, and accuracy. The reduced number of false positive and false negative results is also crucial in detecting brain tumours. It implies that Gabor and GLCM are the best feature extraction algorithms, with DWT coming in a close third. When time spent processing data is taken into account, however, DWT outperforms. Therefore, accuracy in cancer diagnosis is prioritised above computational speed. To enhance the effectiveness of the MRI brain tumour detection system, this study will merge features from Gabor and GLCM. The CSO technique will be

improved. In order to extract the most useful distinguishing features from the techniques, the developed IMCSO will be applied along with the Gabor and GLCM techniques. It is hypothesized that minimizing both false positives and false negatives may be achieved by a synergistic combination of optimal features.

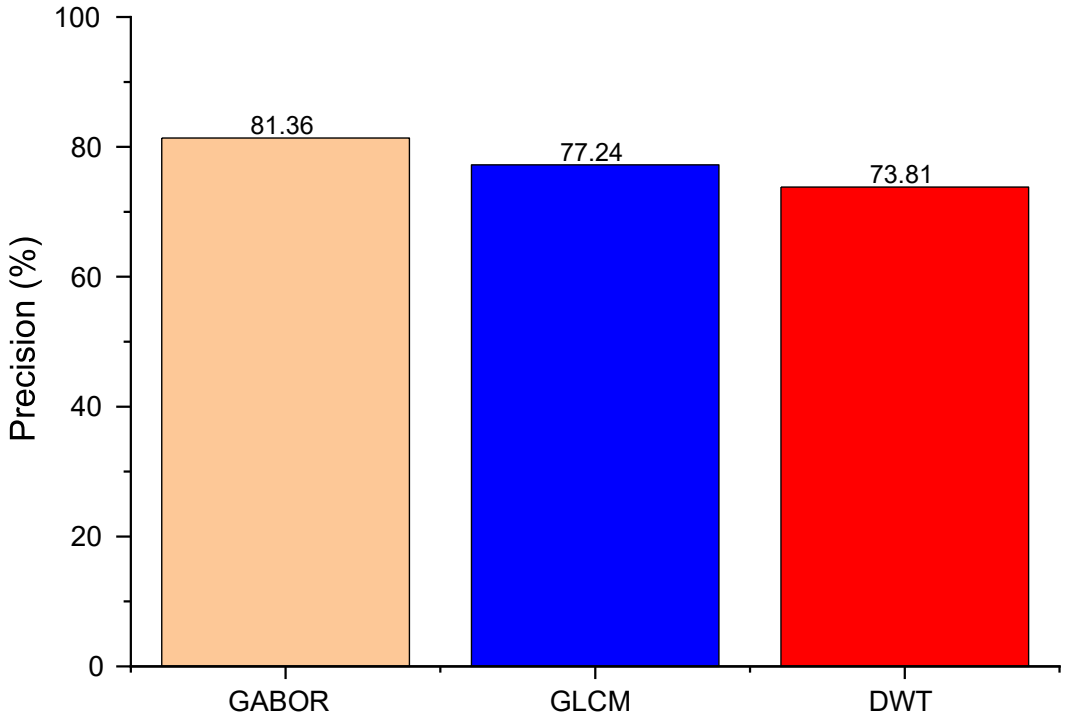


Figure 4.5: Precision Feature Extraction Techniques

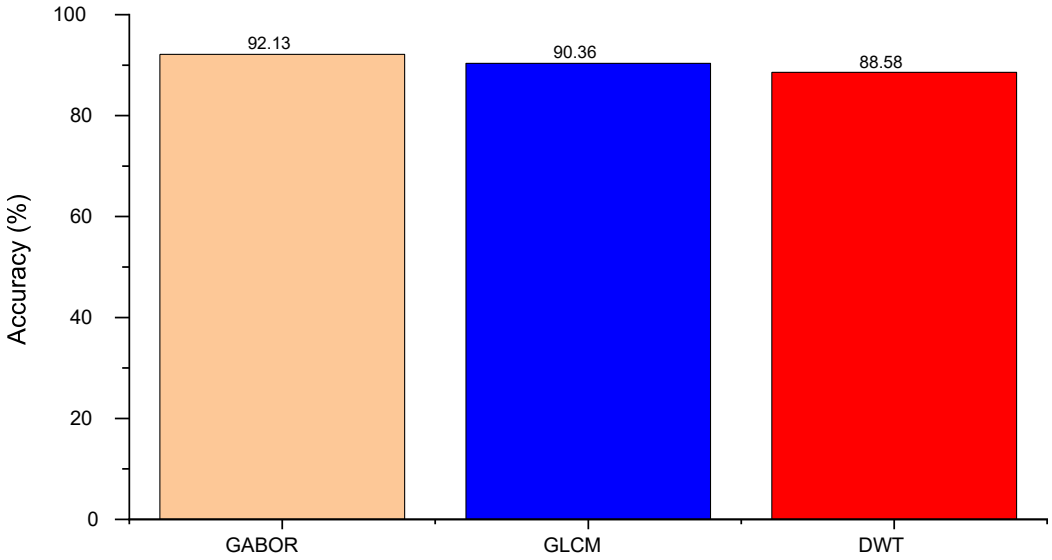


Figure 4.6: Accuracy Feature Extraction Techniques

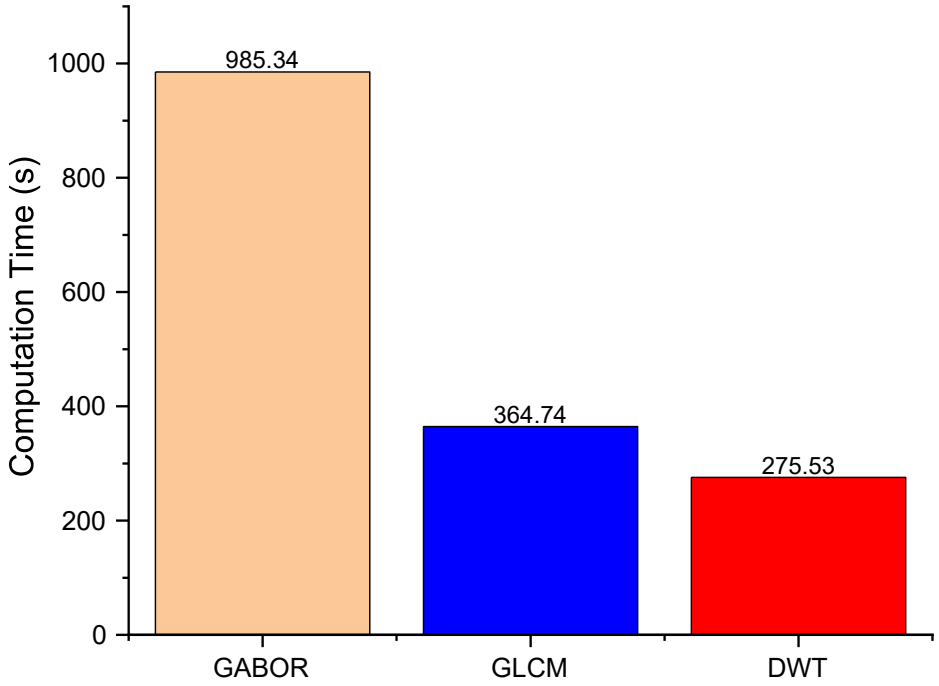


Figure 4.7: Computation time Feature Extraction Techniques

Conclusions

This research work examines the effectiveness of three textural-based feature extraction techniques, namely the Gabor filter, the GLCM, and the DWT, for diagnosing tumours in MRI brain datasets. Gabor features produce fewer false positives and negatives, which influences its accuracy, precision, and sensitivity compared to GLCM and DWT. Furthermore, when compared to the GLCM and DWT features, the Gabor filter was discovered to be computationally expensive. This finding demonstrates that the Gabor filter and GLCM techniques provide a more robust brain MRI computer-aided diagnostic system in terms of accuracy, FPR, FNR, sensitivity, and precision. This is an assertion that combining both techniques would result in a more effective strategy to enhance tumour diagnosis in MRI brain images. Therefore, it is recommended that future work focus on the fusion of feature extraction techniques from selected Garbor filters and GLCM to improve performance. Also, by combining the Gabor filter and GLCM techniques, researchers can leverage the strengths of both methods to create a more accurate and efficient brain MRI computeraided diagnostic system. This fusion of feature extraction techniques has the potential to significantly enhance tumour diagnosis in MRI brain images, making it a promising area for future research and development.

Acknowledgement

The authors gratefully acknowledge the financial support provided by TETFUND for the realization of this research work.

References

Abd-Ellah, M.K., Awad, A.I., Khalaf, A.A.M., and Hamed, H.F.A. (2019). A Review on Brain Tumor Diagnosis from MRI Images: Practical Implications, Key Achievements, and
Lessons Learned. *Magnetic Resonance Imaging*, 300-318. doi:10.1016/j.mri.2019.05.028

Abdusalomov, A.B., Mukhiddinov, M., and Whangbo, T.K. (2023). Brain Tumor Detection Based on Deep Learning Approaches and Magnetic Resonance Imaging. *Cancers,* 15(16), 4172. doi:org/10.3390/cancers15164172

Arulogun, O.T., Falohun, A.S., Ismaila, W.O., and Awokola, J.A. (2016). Performance Analysis of Selected Medical Image Segmentation Algorithms. *International Journal of Computer and Technology,* 15(10), 7140 - 7149.

Balestrino, R., Rudà, R., and Soffietti, R. (2020). Brain Metastasis from Unknown Primary Tumour: Moving from Old Retrospective Studies to Clinical Trials on Targeted Agents.

Cancers, 12(11), 3350. doi:org/10.3390/cancers12113350

Biratu, E.S., Schwenker, F., Ayano, Y.M., and Debelee, T.G. (2021). A Survey of Brain Tumor Segmentation and Classification Algorithms. *Journal of Imaging,* 7(9), 179-209. doi:org/10.3390/jimaging7090179

Deepa, S., Janet, J., Sumathi, S., and Ananth, J.P. (2023). Hybrid Optimization Algorithm Enabled Deep Learning Approach Brain Tumor Segmentation and Classification Using MRI.

Journal of Digital Imaging, 36(3), 847–868. doi:org/10.1007/s10278-022-00752-2

Harati, V., Khayati, R., and Farzan, A. (2011). Fully Automated Tumor Segmentation Based on Improved Fuzzy Connectedness Algorithm in Brain MR Images. *Computers in Biology and Medicine,* 41(7), 483–492. doi:org/10.1016/j.compbiomed.2011.04.010

Ismaila, W.O., Babalola, O.R., Ismaila, F.M., and Ogunjimi, T.O. (2018). Soft Computing: TwoStep Feature Extraction-Based Biometric Authentication System. *International Journal of Emerging Technologies in Computational and Applied Sciences,* 25(1), 22-27.

Kaifi, R. (2023). A Review of Recent Advances in Brain Tumor Diagnosis Based on AI-Based Classification. *Diagnostics (Basel, Switzerland),* 13(18), 3007. doi:org/10.3390/diagnostics13183007

Mahmoud, R.O., Faheem, M.T., and Sarhan, A. (2008). *Intelligent Denoising Technique for Spatial Video Denoising for Real-Time Applications.* Paper presented at the 2008 International Conference on Computer Engineering & Systems.

Raheja, J.L., Kumar, S., and Chaudhary, A. (2013). Fabric Defect Detection Based on GLCM and Gabor filter: A comparison. *Optik - International Journal for Light and Electron Optics,* 124(23), 6469-6474. doi:10.1016/j.ijleo.2013.05.004

Shanthi, A.S., and Karthikeyan, M. (2016). Improving Gabor filter Bank Design and SVM Optimization Using Cuckoo Search For Mild Cognitive Impairment Classification. *Journal of Medical Imaging and Health Informatics,* 6(3), 784-787.

Sung, H., Ferlay, J., Siegel, R.L., Laversanne, M., Soerjomataram, I., Jemal, A., and Bray, F. (2021). Global Cancer Statistics 2020: GLOBOCAN Estimates of Incidence and Mortality Worldwide for 36 Cancers in 185 Countries. *CA: A Cancer Journal for Clinicians,* 71(3), 209–249. doi:org/10.3322/caac.21660

Thakral, S., and Manhas, P. (2018). *Image Processing by using Different Types of Discrete Wavelet Transform.* Paper presented at the International Conference on Advanced Informatics for Computing Research, Singapore.

Ullah, Z., Usman, M., Jeon, M., and Gwak, J. (2022). Cascade Multiscale Residual Attention CNNs with Adaptive ROI for Automatic Brain Tumor Segmentation. *Information Sciences: an International Journal,* 608, 1541-1556.

Wisaeng, K., and Sa-Ngiamvibool, W. (2023). Brain Tumor Segmentation Using Fuzzy Otsu Threshold Morphological Algorithm. *IAENG International Journal of Applied Mathematics,* 53(12), 1-12.

Yamasaki, F. (2022). Adolescent and Young Adult Brain Tumors: Current Topics and Review. *International Journal of Clinical Oncology,* 27(3), 457-464. doi:10.1007/s10147-02102084-7

Yılmaz, A., and Bayrak, G. (2019). A Real-time UWT-based Intelligent Fault Detection Method for PV-based Microgrids. *Electric Power Systems Research,* 177(2019), 105984. doi:10.1016/j.epsr.2019.105984

Zanaty, E.A. . (2012). Determination of Gray Matter (GM) and White Matter (WM) Volume in Brain Magnetic Resonance Images (MRI). *International Journal of Computer Applications,* 45(3), 16–22.